iScience

CellPress
OPEN ACCESS

Article

NLRC4 inhibits NLRP3 inflammasome and abrogates effective antifungal CD8$^+$ T cell responses

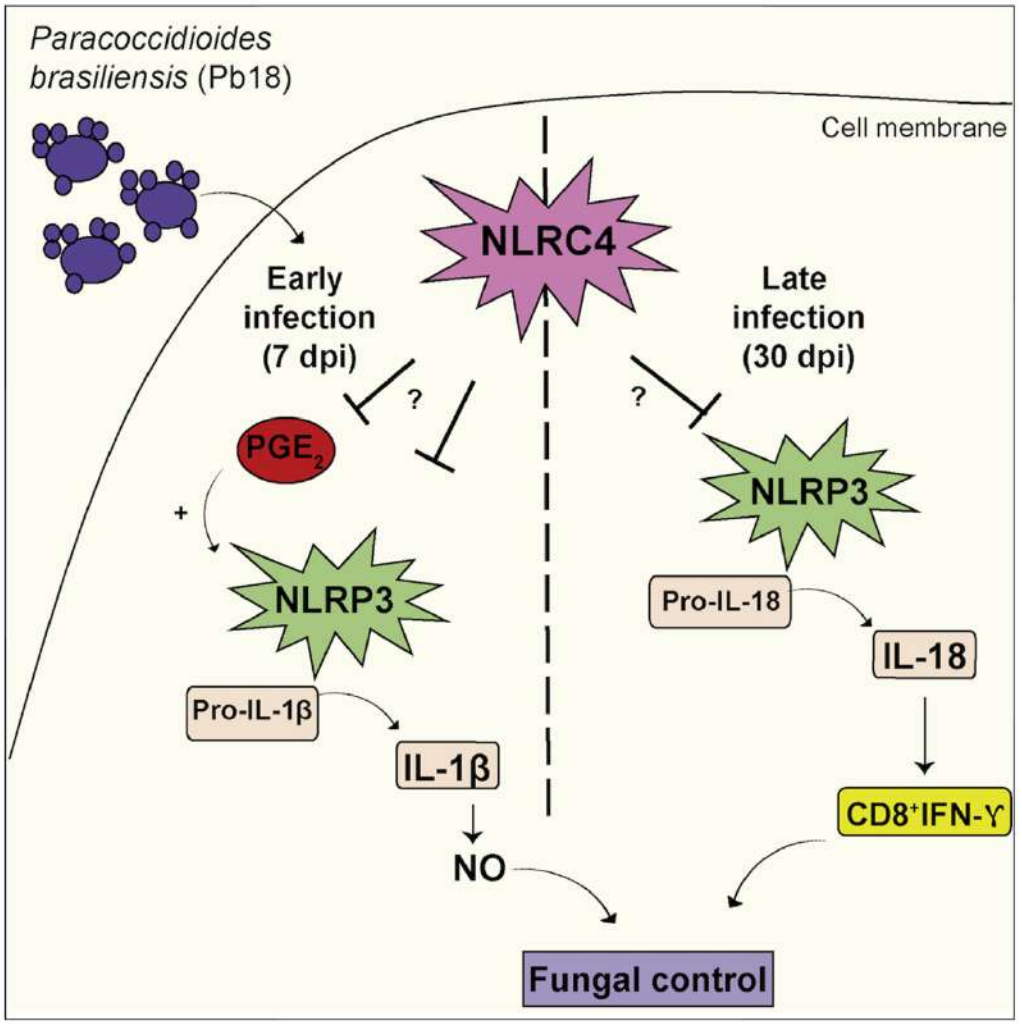

Camila O.S. Souza, Natália Ketelut-Carneiro, Cristiane M. Milanezi, Lúcia H. Faccioli, Luiz G. Gardinassi, João S. Silva

jsdsilva@fmrp.usp.br

Highlights

NLRC4 promotes susceptibility to a highly pathogenic fungus.

NLRC4 regulates NLRP3 activity.

NLRC4 inhibits early NLRP3/IL-1β/NOS2/NO axis and promotes fungal replication.

NLRC4 dampens late IL-18 production, suppressing CD8$^+$IFN-γ$^+$ T cell responses.

Souza et al., iScience 24, 102548
June 25, 2021
https://doi.org/10.1016/j.isci.2021.102548

iScience

CellPress
OPEN ACCESS

Article

NLRC4 inhibits NLRP3 inflammasome and abrogates effective antifungal $CD8^+$ T cell responses

Camila O.S. Souza,[1] Natália Ketelut-Carneiro,[1,2] Cristiane M. Milanezi,[1] Lúcia H. Faccioli,[3] Luiz G. Gardinassi,[4] and João S. Silva[1,5,6,*]

SUMMARY

The recognition of fungi by intracellular NOD-like receptors (NLRs) induces inflammasome assembly and activation. Although the NLRC4 inflammasome has been extensively studied in bacterial infections, its role during fungal infections is unclear. Paracoccidioidomycosis (PCM) is a pathogenic fungal disease caused by *Paracoccidioides brasiliensis*. Here, we show that NLRC4 confers susceptibility to experimental PCM by regulating NLRP3-dependent cytokine production and thus protective effector mechanisms. Early after infection, NLRC4 suppresses prostaglandin E_2 production, and consequently reduces interleukin (IL)-1β release by macrophages and dendritic cells in the lungs. IL-1β is required to control fungal replication via induction of the nitric oxide synthase 2 (NOS2) pathway. At a later stage of the disease, NLRC4 impacts IL-18 release, dampening robust $CD8^+IFN\text{-}\gamma^+$ T cell responses and enhancing mortality of mice. These findings demonstrate that NLRC4 promotes disease by regulating the production of inflammatory cytokines and cellular responses that depend on the NLRP3 inflammasome activity.

INTRODUCTION

Pattern recognition receptors (PRRs) are the frontline of host responses to microbial and danger signals (Bauernfeind and Hornung, 2013; Plato et al., 2015). Concerted efforts of intracellular NOD-like receptors (NLRs) together with an adapter molecule trigger inflammasome assembly, a large multiprotein complex that processes the proinflammatory cytokines interleukin (IL)-1β/IL-18 and induces cell death (Ketelut-Carneiro and Fitzgerald, 2020; Martinon et al., 2002). Inflammasome activity has been linked to opportunistic fungal infection (Tavares et al., 2015). Paracoccidioidomycosis (PCM) is a severe human disease caused by the fungi of the genus *Paracoccidioides* (Franco, 1987). The infection initiates in the lungs, where it causes a chronic granulomatous inflammation, but can disseminate through circulatory and lymphatic systems (Calich et al., 1998; Martinez, 2017). The intracellular receptor NLRP3 has been studied during experimental infections with *P. brasiliensis* (Feriotti et al., 2017; Ketelut-Carneiro et al., 2015; Tavares et al., 2013). NLRP3 inflammasome assembly and caspase-1 activation mediates IL-1β and IL-18 maturation, while inducing pyroptotic cell death (He et al., 2016). After *P. brasiliensis* infection, *Nlrp3*$^{-/-}$ mice harbor increased fungal burdens and succumb to disease owing to a failure in IL-18 production that amplifies Th1 immunity during PCM (Calich et al., 1998; Ketelut-Carneiro et al., 2015). NLRP3 is also required for IL-1β release during *P. brasiliensis* infection *in vivo* (Feriotti et al., 2017). However, the role of other NLRs during PCM remains elusive.

NLRC4 is an intracellular PRR that recognizes flagellin via an NAIP-dependent mechanism (Amer et al., 2006; Andrade and Zamboni, 2020; Mariathasan et al., 2004; Sutterwala et al., 2007). NLRC4 inflammasome activation is regulated by diverse factors, including bioactive lipids (Pedraza-Alva et al., 2015; Tang et al., 2018). A recent study suggests that prostaglandin (PG) E_2-EP3 receptor signaling leads to NLRC4 inflammasome assembly after incubation with *Anaplasma phagocytophilum* (Wang et al., 2016). Moreover, activation of NLRC4 inflammasome in intestinal epithelial cells coordinates innate immune responses involving a local PGE_2 release and IL-18 production (Rauch et al., 2017). Other bacterial molecules also trigger NLRC4 inflammasome activation, suggesting a broader role for this receptor beyond flagellin sensing (Miao et al., 2010; Suzuki et al., 2007). NLRC4 is necessary for IL-1β and IL-18 production and leukocyte recruitment to

[1]Department of Biochemistry and Immunology, Ribeirão Preto Medical School, University of São Paulo, Ribeirão Preto, SP, Brazil

[2]Program in Innate Immunity, Department of Medicine, University of Massachusetts Medical School, Worcester, MA 01605, USA

[3]Department of Clinical Analyses, Toxicology and Bromatological Science, School of Pharmaceutical Sciences of Ribeirão Preto, University of São Paulo, Ribeirão Preto, SP, Brazil

[4]Department of Biosciences and Technology, Institute of Tropical Pathology and Public Health, Federal University of Goiás, Goiânia, GO, Brazil

[5]Fiocruz-Bi-Institutional Translational Medicine Platform, Ribeirão Preto, SP, Brazil

[6]Lead contact

*Correspondence: jsdsilva@fmrp.usp.br

https://doi.org/10.1016/j.isci.2021.102548

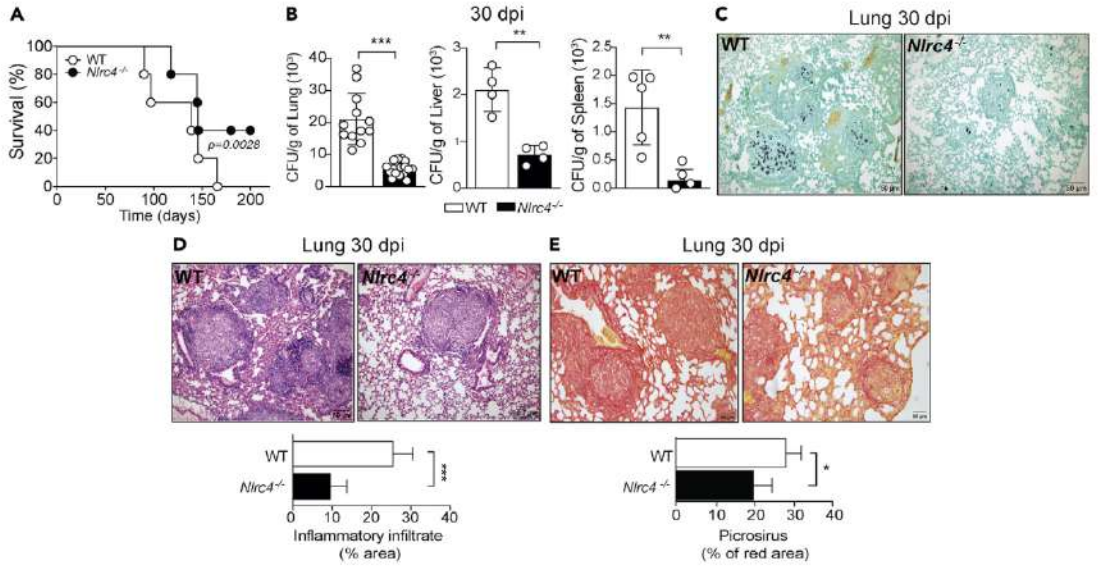

Figure 1. Pathogenic activity of NLRC4 during experimental PCM

C57BL/6 (WT) and *Nlrc4*$^{-/-}$ mice were intravenously infected with 1x10^6 viable Pb18 yeasts

(A) Line plots show the percentage of survival of WT and *Nlrc4*$^{-/-}$ mice. Animals were monitored daily for 200 days (n = 5 mice/group). **p < 0.0028 using log rank test of one experiment.

(B) Scatterplots with bars show the fungal load in the lungs, liver, and spleen of WT and *Nlrc4*$^{-/-}$ mice at 30 dpi.

(C) *P. brasiliensis* was stained in the lungs of mice at 30 dpi using the Grocott method.

(D) Histological sections of lungs from WT and *Nlrc4*$^{-/-}$ mice at 30 dpi using H&E staining. Bar graphs show the percentage of inflammatory infiltrate.

(E) Lung sections from WT and *Nlrc4*$^{-/-}$ mice at 30 dpi using the picrosirius red staining. Bar graphs show the percentage of red area. All photomicrography was analyzed using a light microscope, scale bar: 50 μm (n = 9–10 WT and 9–13 *Nlrc4*$^{-/-}$ Pb18-infected mice). Error bars depict mean ± SD. Results represent a pool of three independent experiments. Statistically significant differences were evaluated with unpaired t test (*p < 0.05, **p < 0.01, ***p < 0.001 compared with WT in each time point).

the oral mucosa during infection with *Candida albicans* (Tomalka et al., 2011). Furthermore, NLRC4 promotes IL-1 receptor antagonist (IL-1Ra) production, which regulates a pathogenic NLRP3 activity during vulvovaginal candidiasis (Borghi et al., 2015). We, therefore, hypothesized that NLRC4 deficiency would confer susceptibility in a mouse model of PCM. Unexpectedly, NLRC4 deficiency resulted in enhanced resistance to systemic *P. brasiliensis* infection. This phenotype resulted from improved NLRP3 inflammasome activity and robust CD8$^+$IFN-γ$^+$ T cell response in the lungs. Collectively, these data demonstrate that NLRC4 prevents an effective NLRP3-dependent antifungal immune response during PCM.

RESULTS

NLRC4 confers susceptibility to experimental PCM

To investigate the role of NLRC4 during experimental PCM, wild-type (WT) and *Nlrc4*$^{-/-}$ mice were infected intravenously with 1x10^6 Pb18 yeast cells and the survival rate was monitored for 200 days. Compared with controls, *Nlrc4*$^{-/-}$ mice exhibited enhanced resistance to fatal outcome (Figure 1A). Fungal burdens were significantly lower in the lungs, liver, and spleen of *Nlrc4*$^{-/-}$ mice 30 days post infection (dpi) (Figure 1B). Grocott staining of infected lungs confirmed this phenotype (Figure 1C). Thus, these results suggest that despite the *P. brasiliensis* tropism to the lungs (Tristão et al., 2013), *Nlrc4*$^{-/-}$ mice are systemically resistant to *P. brasiliensis* infection. Thirty dpi, histopathological analyses of lungs from infected mice demonstrated a significant reduction of the inflammatory infiltrate in *Nlrc4*$^{-/-}$ mice compared with controls (Figure 1D). Collagen deposition was also reduced (Figure 1E). These data provide evidence for a pathogenic role of NLRC4 during experimental PCM.

NLRC4 inhibits IL-1β at early stages of *P. brasiliensis* infection

NLRC4 inflammasome activation is crucial for IL-1β production, which has fungicidal activity against *C. albicans* (Tomalka et al., 2011). To address whether NLRC4 activation induces protection against *P. brasiliensis* early after infection, WT and *Nlrc4*$^{-/-}$ mice were infected and the colony-forming unit

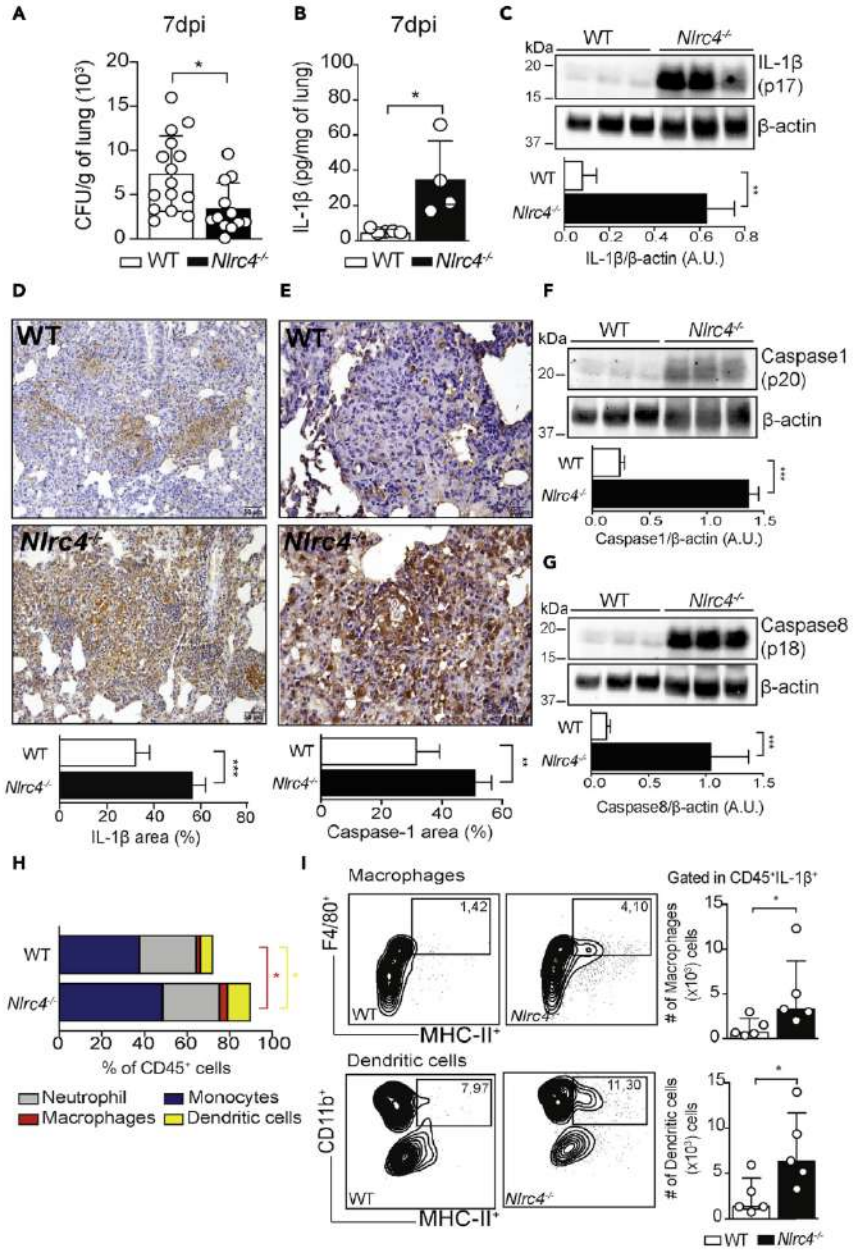

Figure 2. NLRC4 regulates early IL-1β release after *P. brasiliensis* infection

WT and *Nlrc4*$^{-/-}$ and mice were intravenously infected with 1x10^{6} of viable Pb18 yeasts.

(A) Scatterplots with bars show the fungal load in lung of WT and *Nlrc4*$^{-/-}$ mice at 7 dpi. Results represent a pool of three independent experiments.

(B) Scatterplots with bars show the quantification of IL-1β at 7 in the lungs of WT and *Nlrc4*$^{-/-}$ mice.

(C) Western blotting analysis detecting IL-1β cleavage (p17) in lung homogenates from WT and *Nlrc4*$^{-/-}$ mice at 7 dpi. The intensities of IL-1β protein were quantified using iBright™ CL1500 Imaging System.

(D) IL-1β expression was visualized in the lungs of mice at 7 dpi from both groups using immunohistochemistry (Scale bar: 50 μM – left panel). Each column represents the mean ± SD.

(E) Caspase-1 expression was visualized in the lungs of mice at 7 dpi from both groups using immunohistochemistry (Scale bar: 20 μM – right panel). Each column represents the mean ± SD.

(F) Active caspase-1 (p20) was detected by Western blotting in the lungs from WT and *Nlc4*$^{-/-}$ mice at 7 dpi. The intensities of active caspase-1 were quantified using iBright™ CL1500 Imaging System.

(G) Active caspase-8 (p18) was detect by Western blotting in the lungs from WT and *Nlc4*$^{-/-}$ mice at 7 dpi. The intensities of active caspase-8 were quantified using iBright™ CL1500 Imaging System.

Figure 2. *Continued*

(H) Stacked bars show the percentage of neutrophils (Ly6G$^+$ CD11b$^+$), monocytes (Ly6G$^-$, Ly6C$^+$ CD11b$^+$), macrophages (CD11b$^+$F4/80$^+$MHC-II$^+$), and dendritic cells (CD11c$^+$CD11b$^+$MHC-II$^+$).

(I) Contour plots show representative flow cytometric data and scatterplots with bars show the absolute numbers of macrophages and dendritic cells gated in CD45$^+$IL-1β$^+$ cells at 7 dpi (n = 5 infected mice per group at 7 dpi).Data represent one of two independent experiments (n = 3–5 infected mice per group at each time point). Data are expressed as mean ± SD. Statistically significant differences were evaluated with ANOVA followed by Bonferroni's multiple comparisons test or unpaired t-test (*p < 0.05, **p < 0.01, ***p < 0.001).

See also Figure S1.

(CFU) was analyzed at 7 and 15 dpi. NLRC4 deficiency reduced CFU counts in the lungs at 7 dpi (Figure 2A), but there were not significant changes at 15 dpi (see Figure S1A). In addition, we quantified IL-1β at 7, 15, and 30 dpi. Compared with WT animals, levels of IL-1β increased in the lungs of *Nlrc4*$^{-/-}$ mice at 7 dpi, but there were no differences at 15 dpi (see Figure S1B) and 30 dpi (see Figure S1C). As enzyme-linked immunosorbent assay detects both pro-IL-1β and cleaved IL-1β, we evaluated the presence of the active form of IL-1β by Western blot. At 7 dpi, mature IL-1β (p17 subunit) was abundantly found in the lungs from Pb18-infected *Nlrc4*$^{-/-}$ but not from WT mice (Figure 2C). Immunohistochemical analysis confirmed these results *in situ* by showing that infected *Nlrc4*$^{-/-}$ animals expressed high levels of pulmonary IL-1β after 7 dpi (Figure 2D). Corroborating these findings, the elevated levels of IL-1β in the lungs of Pb18-infected *Nlrc4*$^{-/-}$ mice correlated with increased caspase-1 expression (Figure 2E) and activation (Figure 2F). We previously demonstrated caspase-8 as an additional pathway for IL-1β cleavage in response to *P. brasiliensis* infection (Ketelut-Carneiro et al., 2018). Interestingly, *P. brasiliensis* infection also promoted caspase-8 (p18 subunit) activation in the lungs of *Nlrc4*$^{-/-}$ mice at 7 dpi (Figure 2G). Therefore, NLRC4 inhibits caspase-1 and caspase-8 activation, leading to reduced IL-1β processing and subsequent uncontrolled fungal burden at an early stage of infection.

Next, we determined the leukocyte population that produces IL-1β in Pb18-infected *Nlrc4*$^{-/-}$ mice at 7 dpi, applying the flow cytometric gating hierarchy shown in Figure S1 D. Compared with WT animals, the frequency and number of macrophages and dendritic cells (DCs) increased in the lungs of *Nlrc4*$^{-/-}$ mice, but we did not observe significant changes in monocytes and neutrophils (Figure 2H and see Figure S1E). Both, macrophages and DCs were the main source of IL-1β (Figure 2I and Figure S1F). Taken together, these data show that macrophages and DCs release IL-1β in the lungs of *Nlrc4*$^{-/-}$ mice at the early stage of *P. brasiliensis* infection.

NLRC4 affects the IL-1β/NOS2/NO-dependent fungicidal mechanism

Because macrophages produce IL-1β during the initial stage of Pb18 infection in the lungs of *Nlrc4*$^{-/-}$ mice, we used bone-morrow-derived macrophages (BMDMs) to determine whether NLRC4 impacts IL-1β production *in vitro*. Of note, Pb18-infected *Nlrc4*$^{-/-}$ BMDMs increased secretion of IL-1β when compared with WT and *Nlrp3*$^{-/-}$ BMDMs (Figure 3A). Indeed, levels of mature IL-1β (p17 subunit) were higher in supernatants of *Nlrc4*$^{-/-}$ BMDMs, whereas p17 subunit was absent in supernatants of *Nlrp3*$^{-/-}$ BMDMs (Figure 3B). Tumor necrosis factor alpha secretion remained unaffected (Figure 3C). Collectively, these data demonstrate that NLRC4 activation regulates IL-1β release after incubation of BMDMS with Pb18.

Previous studies demonstrated that IL-1β and interferon (IFN)-γ promote killing of *P. brasiliensis* yeast (Kurita et al., 2005). We also observed elevated fungal load in WT BMDMs, which decreased significantly after pretreatment with rIFN-γ (Figure 3D). Importantly, NLRC4 deficiency enhanced the fungicidal activity of BMDMs, which was comparable with that of WT cells pretreated with rIFN-γ (Figure 3D). Furthermore, the addition of rIL-1β to WT BMDMs improved their ability to kill *P. brasiliensis* yeasts, whereas neutralization of IL-1β in *Nlrc4*$^{-/-}$ BMDMs reduced the ability of these cells to restrain fungal growth (Figure 3E).

Both IL-1β and IFN-γ signaling induce the nitric oxide synthase 2 (NOS2) pathway and production of NO by macrophages (Brummer et al., 1988; Ketelut-Carneiro et al., 2019; Lima-Junior et al., 2013). Indeed, *Nlrc4*$^{-/-}$ BMDMs incubated with Pb18, which release high levels of IL-1β, produced higher levels of NO when compared to WT cells (Figure 3F), which was reduced after IL-1β neutralization (Figure 3G). NO has a protective role in PCM (Gonzalez et al., 2000). In accordance, higher CFU counts were detected after incubating Pb18-infected BMDMs from both groups with aminoguanidine, an endogenous NO inhibitor (Figure 3H). Supporting these data, we identified upregulated expression of *Nos2* in the lungs of Pb18-infected *Nlrc4*$^{-/-}$ mice at 7 dpi (see Figures S2A and S2B). To discard the potential role of IFN-γ in triggering NO

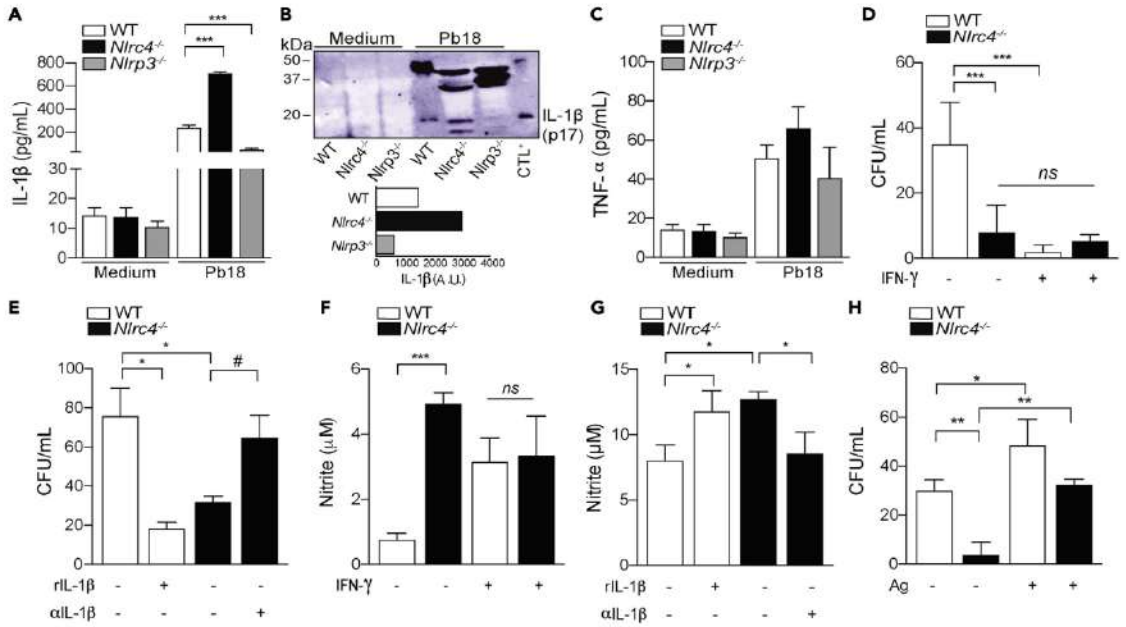

Figure 3. NLRC4 inhibits IL-1β and NO release by BMDMs incubated with *P. brasiliensis*

(A and B) BMDMs ($2x10^5$ for ELISA and Griess assay or $2x10^6$ for Western blotting) from WT, *Nlrc4*$^{-/-}$ and *Nlrp3*$^{-/-}$ mice were incubated at MOI 5 for 48 h. (A) Supernatants were used to quantify levels of IL-1β by ELISA. (B) Active form of IL-1β (p17) was determined by Western blotting. WT BMDMs primed with LPS (500ng/mL) and nigericin (20uM) were used as a positive control for the secretion of p17 subunit. The intensities of IL-1β protein were quantified using ImageJ software.

(C) TNF-α was quantified in cell supernatants after 48 hr

(D) BMDMs ($2.5x10^5$) from WT and *Nlrc4*$^{-/-}$ mice were pretreated with rIFN-γ (50 ng/mL) overnight, followed by Pb18 incubation at MOI 25:1. After 48 h of incubation, BMDMs were washed, lysed, and plated in BHI for quantification of fungal growth.

(E) Fungal load in WT and *Nlrc4*$^{-/-}$ BMDMs stimulated with rIL-1β (20ng/mL) or αIL-1β (20ng/mL) overnight.

(F) Supernatants of BMDMs from WT and *Nlrc4*$^{-/-}$ cultured with rIFN-γ (50 ng/mL) were collected to measure the levels of nitrite by Griess method.

(G) Supernatants of WT or *Nlrc4*$^{-/-}$ BMDMs cultured with rIL-1β (20ng/mL) or αIL-1β (20ng/mL) were collected to measure the levels of nitrite by Griess assay.

(H) Fungal growth was quantified in WT and *Nlrc4*$^{-/-}$ BMDMs infected with *P. brasiliensis* (MOI 25:1) and cultured or not with aminoguanidine (Ag. 1mM) overnight. Data represent one of two independent experiments using triplicates. Results are expressed as mean ± SD. Statistically significant differences were evaluated with ANOVA followed by Bonferroni's multiple comparisons test (#) $p < 0.05$ compared to *Nlrc4*$^{-/-}$ BMDMs not treated with αIL-1β. (*$p < 0.05$, **$p < 0.01$, ***$p < 0.001$).

See also Figure S2.

synthesis at the beginning of the infection, we quantified IFN-γ in lung homogenates. There were no differences in the levels of this cytokine (see Figure S2C), indicating that NLRC4-induced IL-1β plays a role in controlling fungal growth early after infection. Taken together, the data reveal that NLRC4 disrupts the IL-1β/NOS2/NO pathway in response to *P. brasiliensis* infection.

NLRC4-dependent PGE_2 suppression regulates IL-1β release during PCM

Previous studies showed that NLRP3 inflammasome is required for efficient control of *P. brasiliensis* infection (Feriotti et al., 2017; Ketelut-Carneiro et al., 2015; Tavares et al., 2013). Therefore, we investigated whether NLRC4 might impact NLRP3 activity. Compared with WT mice, NLRC4 deficiency resulted in significant upregulation of *Nlrp3* at 7 and 30 dpi (Figure 4A). In addition, *Nlrc4*$^{-/-}$ BMDMs enhanced *Nlrp3* expression after incubation with Pb18 for 2, 6, and 12 h (see Figure S3A). Because NLRC4 inhibits NLRP3 via IL-1Ra during *C. albicans* infection (Borghi et al., 2015), we investigated whether a similar mechanism occurs in PB18-infected *Nlrc4*$^{-/-}$ mice. Similar amounts of IL-1Ra were detected in the lungs of WT and *Nlrc4*$^{-/-}$ mice at 7 and 30 dpi (see Figure S3B). Collectively, these results suggest that NLRC4 inhibits NLRP3 inflammasome activity along the course of *P. brasiliensis* infection via an IL-1Ra-independent mechanism.

Cyclooxygenase (COX)-2 is a rate-limiting enzyme for prostaglandin biosynthesis, which has been associated with NLRC4 (Rauch et al., 2017; Sokolowska et al., 2015; von Moltke et al., 2012) and NLRP3 (Hua et al.,

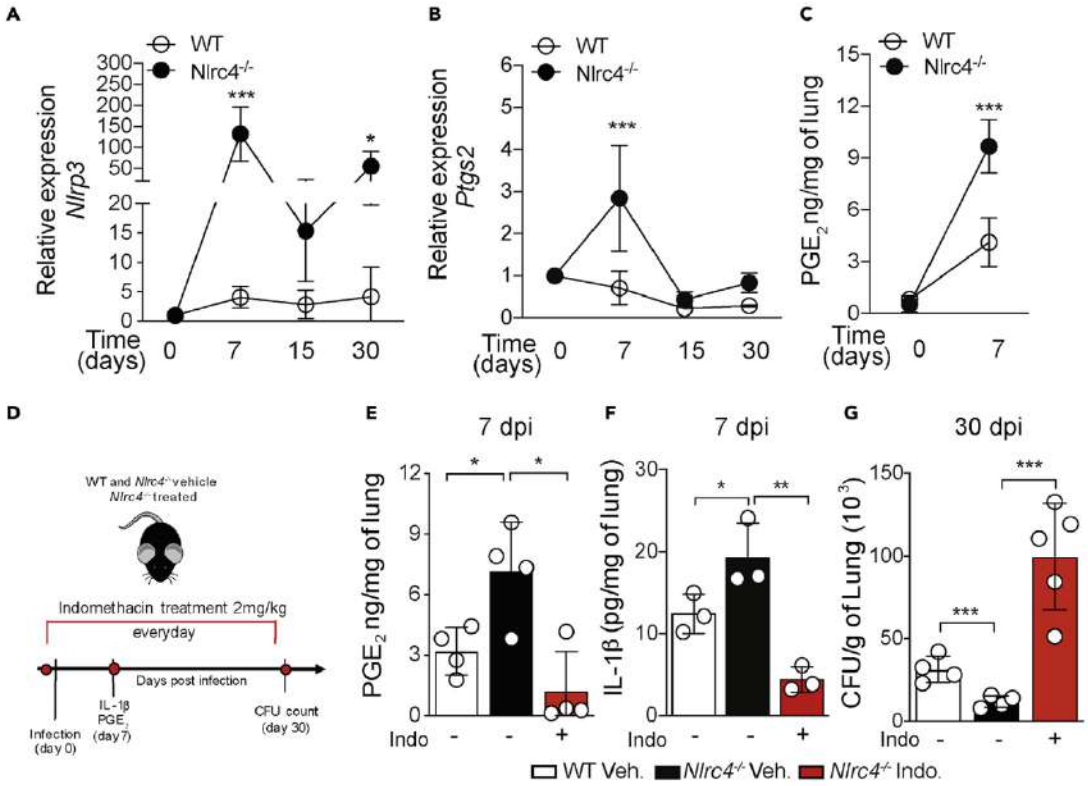

Figure 4. NLRC4-dependent PGE_2 suppression promotes *P. brasiliensis* replication

WT and *Nlrc4*$^{-/-}$ mice were intravenously infected with 1x10^6 of viable Pb18 yeasts and the lungs were collected at 7, 15, and 30 dpi.

(A) Line plots show the kinetics of *Nlrp3* expression in WT and *Nlrc4*$^{-/-}$ mice before and during 30 days of infection with Pb18.

(B) Line plots show the kinetics of *Ptgs2* (cyclooxygenase-2) expression in the lungs along the course of Pb18 infection. Data represent one of two independent experiments performed with triplicates.

(C) Line plots show PGE_2 quantification by LC-MS/MS in the lungs of mice of both groups at 7 dpi.

(D) Schematic representation of the treatment with indomethacin.

(E) Scatterplots with bars show the quantification of PGE_2 by LC-MS/MS at 7 dpi.

(F) Scatterplots with bars show the quantification of IL-1β by ELISA at 7 dpi.

(G) CFU counting in the lungs from WT and *Nlrc4*$^{-/-}$ mice treated or not with indomethacin (2mg/kg) after 30 days of infection with 1x10^6 Pb18 yeasts. Data represent one independent experiment (n= 3–4 WT or *Nlrc4*$^{-/-}$ control mice and n = 3-5 *Nlrc4*$^{-/-}$ indomethacin-treated mice per group and time point). Data are expressed as mean ± SD. Statistically significant differences were evaluated with ANOVA followed by Bonferroni's multiple comparisons test (*$p < 0.05$, **$p < 0.01$, ***$p < 0.001$).

See also Figure S3.

2015; Zoccal et al., 2016) inflammasome activities. Compared with WT BMDMs, we observed the upregulation of *Ptgs2* (COX-2 gene) expression in *Nlrc4*$^{-/-}$ cells at 4 and 24 h of incubation with Pb18 (see Figure S3C). Furthermore, *Ptgs2* was also upregulated in the lungs of *Nlrc4*$^{-/-}$ mice after 7 days of *P. brasiliensis* infection (Figure 4B). Corroborating these data, levels of PGE_2 increased significantly in the lungs of *Nlrc4*$^{-/-}$ mice at 7 dpi (Figure 4C) but remained similar to that of WT mice at 15 and 30 dpi (see Figure S3D). To investigate whether NLRC4 impacts NLRP3 activity and resistance to infection via a COX-2/PGE_2-dependent mechanism, we pretreated BMDMs with both a nonselective COX inhibitor (indomethacin) and a selective PGE2 synthase-1 inhibitor (CAY10526) before the infection. *Nlrc4*$^{-/-}$ BMDMs incubated with Pb18 secreted significantly more IL-1β, but there was a striking reduction in IL-1β production after indomethacin (see Figure S3E) and CAY10526 (see Figure S3F) treatment in cells from both groups. Moreover, the selective inhibition of PGE_2 biosynthesis also abrogated Nlrp3 expression in BMDMs from both groups after 12 h of incubation with Pb18 (see Figure S3G), while the CFU counts increased in CAY10526-treated *Nlrc4*$^{-/-}$ BMDMs, but not in WT cells (see Figure S3H).

To confirm that NLRC4 downregulates PGE_2 and this affects IL-1β production and resistance to *P. brasiliensis* infection, we infected *Nlrc4*$^{-/-}$ and WT mice and treated them with indomethacin as per

the experimental design provided in Figure 4D. Indomethacin abrogated PGE_2 production (Figure 4E) and reduced the levels of IL-1β in the lungs of *Nlrc4*$^{-/-}$ mice at 7 dpi (Figure 4F). Furthermore, we observed a striking increase of fungal burden in the lungs of *Nlrc4*$^{-/-}$ mice treated with indomethacin when compared with nontreated *Nlrc4*$^{-/-}$ mice at 30 dpi (Figure 4G). These data indicate that NLRC4 significantly blocks PGE_2 production, which is necessary for IL-1β production at 7 days after *P. brasiliensis* infection. Collectively, these data suggest that early after infection, NLRC4 blocks PGE_2 biosynthesis, which is required to enhance the transcription of *Nlrp3*, to increase the secretion of IL-1β, and to promote a better control of fungal replication.

To assess the biological function of PGE_2 in regulating fungicidal mechanisms, we pretreated WT BMDMs with either rIFN-γ or PGE_2. Treatment with PGE_2 led to effective fungal clearance, which was comparable with that of WT cells pretreated with rIFN-γ (see Figure S3I). It has been demonstrated that both host cells (Balderramas et al., 2014) and *P. brasiliensis* itself could be a source of PGE_2 (Bordon et al., 2007). Because we detected the augment of PGE_2 and higher levels of IL-1β in *Nlrc4*$^{-/-}$ mice infected with *P. brasiliensis*, we next confirmed whether the IL-1β production triggered by PGE_2 was because of fungal replication in the host cells. While live *P. brasiliensis* induced IL-1β secretion in WT macrophages, heat-killed *P. brasiliensis* did not alters IL-1β levels even after addition of exogenous PGE_2 (see Figure S3J). Taken together, these data confirm that live *P. brasiliensis* is required to induce PGE_2-dependent IL-1β release by host cells.

NLRC4 dampens CD8$^+$T cell-mediated IFN-γ response to *P. brasiliensis* infection

During *C. albicans* infection, NLRC4 activation induces IL-1β release and coordinates the development of Th17 immunity and neutrophil recruitment (Tomalka et al., 2011). Although Th17 cells are protective during experimental PCM (Tristão et al., 2017), there were no significant alterations on the levels of Th17-associated cytokines/chemokines in the lungs of Pb18-infected *Nlrc4*$^{-/-}$ mice after 30 dpi (see Figure S4A). Instead, the levels of IL-12p40 and IL-18 were increased in the lungs of *Nlrc4*$^{-/-}$ mice at 30 dpi (Figure 5A). Considering that IL-12 and IL-18 are potent inducers of IFN-γ production, which protects against *P. brasiliensis* infection (Calich et al., 1998; Ketelut-Carneiro et al., 2015), we hypothesized that higher IL-18 production in the lungs of *Nlrc4*$^{-/-}$ mice would promote resistance to *P. brasiliensis* owing to an enhancement of Th1 immunity. Compared with controls, levels of IFN-γ increased, whereas those of IL-10 diminished in the lungs of *Nlrc4*$^{-/-}$ mice at 30 dpi (Figure 5B). These results suggest that NLRC4 also inhibits NLRP3 inflammasome at later stages of *P. brasiliensis* infection, whereas NLRP3 activity is required for a robust Th1 response and IFN-γ production.

After activation, NLRP3 recruits the adapter molecule ASC to trigger the assembly of inflammasome platform (Ketelut-Carneiro and Fitzgerald, 2020; Martinon et al., 2002). To explore whether NLRC4 indeed abrogates the protective IFN-γ response via inhibition of NLRP3 activity, we infected WT and double-knockout *Nlrc4*$^{-/-}$ *Asc*$^{-/-}$ mice with $1x10^6$ viable yeast of *P. brasiliensis*. Compared with WT mice, *Nlc4*$^{-/-}$ *Asc*$^{-/-}$ animals exhibited higher CFU counts (see Figure S5A) and increased inflammatory infiltrate (see Figure S5B), but similar amounts of IFN-γ in the lungs at 30 dpi (see Figure S5C). These data support the hypothesis that an intact NLPR3 inflammasome platform is required for the enhancement of IFN-γ production by *Nlrc4*$^{-/-}$ mice at later stages of *P. brasiliensis* infection.

Furthermore, we explored the impact of NLRC4 over the development of the adaptive immune response to *P. brasiliensis*, applying the flow cytometric gating hierarchy shown in Figure S4 B. The analysis revealed similar frequencies and numbers of CD3$^+$CD4$^+$IFN-γ$^+$ T cells in the lungs of WT and *Nlrc4*$^{-/-}$ mice (Figure 5C). Importantly, both frequency and numbers of CD3$^+$CD8$^+$IFN-γ$^+$ T cells increased significantly in the lungs of *Nlrc4*$^{-/-}$ mice (Figure 5D). Moreover, there were increased numbers of CD8$^+$ T cells producing perforin and granzyme-B, but not granzyme-A, in the lung of Pb18-infected *Nlrc4*$^{-/-}$ animals (Figure 5E). To validate these findings and establish that NLRC4 operates via inhibition of NLRP3 inflammasome to dampen Th1 immunity, we treated *P. brasiliensis*-infected WT and *Nlrc4*$^{-/-}$ mice with MCC950, a selective pharmacological inhibitor of NLRP3, as per the experimental design in Figure 6A. As expected, MCC950-treated *Nlrc4*$^{-/-}$ mice harbored more fungi (Figure 6B) and exhibited decreased pulmonary levels of IL-18 (Figure 6C) and IFN-γ (Figure 6D) in the lungs at 30 dpi. Strikingly, the frequency of CD8$^+$IFN-γ$^+$ T cells was impaired (Figure 6E). Taken together, these data demonstrate that NLRC4 inhibits the NLRP3 inflammasome, which in turn, mitigates the development of antifungal CD8$^+$IFN-γ$^+$ T cell responses.

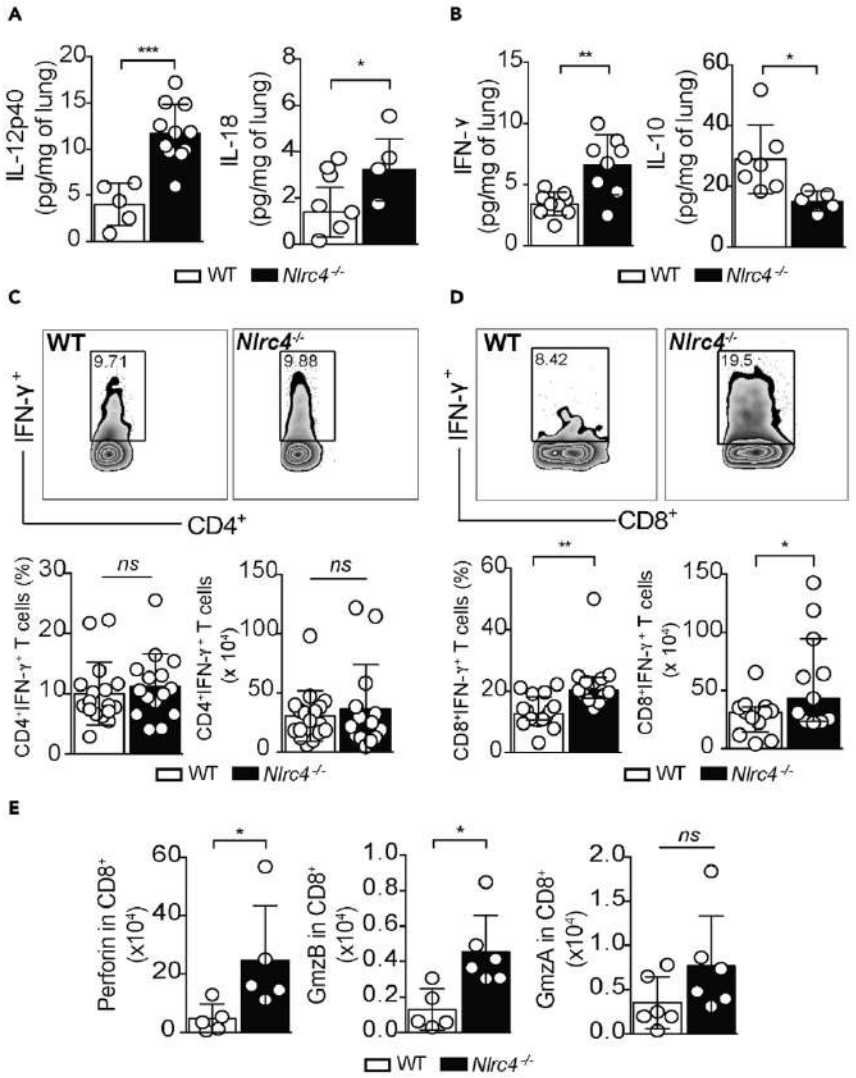

Figure 5. NLRC4 deficiency promotes robust CD8$^+$ T cell responses during PCM

WT and *Nlrc4*$^{-/-}$ mice were intravenously infected with 1x10^6 viable Pb18 yeasts.

(A) Scatterplot with bars show the quantification of IL-12p40 and IL18 at 30 dpi.

(B) Scatterplot with bars show the quantification of IFN-γ and IL-10 in lungs at 30 dpi.

(C) Contour plots represent flow cytometry data of CD4$^+$IFN-γ$^+$ T cells and scatterplots with bars show the percentage and absolute number of CD4$^+$IFN-γ$^+$ T cells.

(D) Contour plots represent flow cytometry data of CD8$^+$IFN-γ$^+$ T cells and scatterplots with bars show the percentage and absolute number of CD8$^+$IFN-γ$^+$ T cells. Results represent a pool of three independent experiment (n = 11–14 infected mice WT or *Nlrc4*$^{-/-}$).

(E) Scatterplots with bars show the absolute number of CD8$^+$ perforin$^+$; CD8$^+$ granzyme-B$^+$, and CD8$^+$ granzyme-A$^+$ T cells. Data represent one independent experiment (n= 4-6 WT or *Nlrc4*$^{-/-}$ mice per group). Error bars depict mean ± SD. Statistically significant differences were evaluated with unpaired t test (*p < 0.05, **p < 0.01, ***p < 0.001).

See also Figures S4 and S5.

DISCUSSION

Our study revealed that NLRC4 confers susceptibility to experimental infection with *P. brasiliensis*. *Nlrc4*$^{-/-}$ mice survived more, controlled fungal replication more efficiently and had reduced inflammatory infiltrate and fibrosis in the lungs during later stages of infection. Compelling findings with *C. albicans* (Joly et al., 2009) and *Aspergillus fumigatus* (Iannitti et al., 2016) showed that NLRC4 inflammasome activation dampens IL-1β production. Our study demonstrates that NLRC4 affects the activity of caspase-1 and caspase-8, which correlates with low levels of IL-1β early after *P. brasiliensis* infection. We have demonstrated

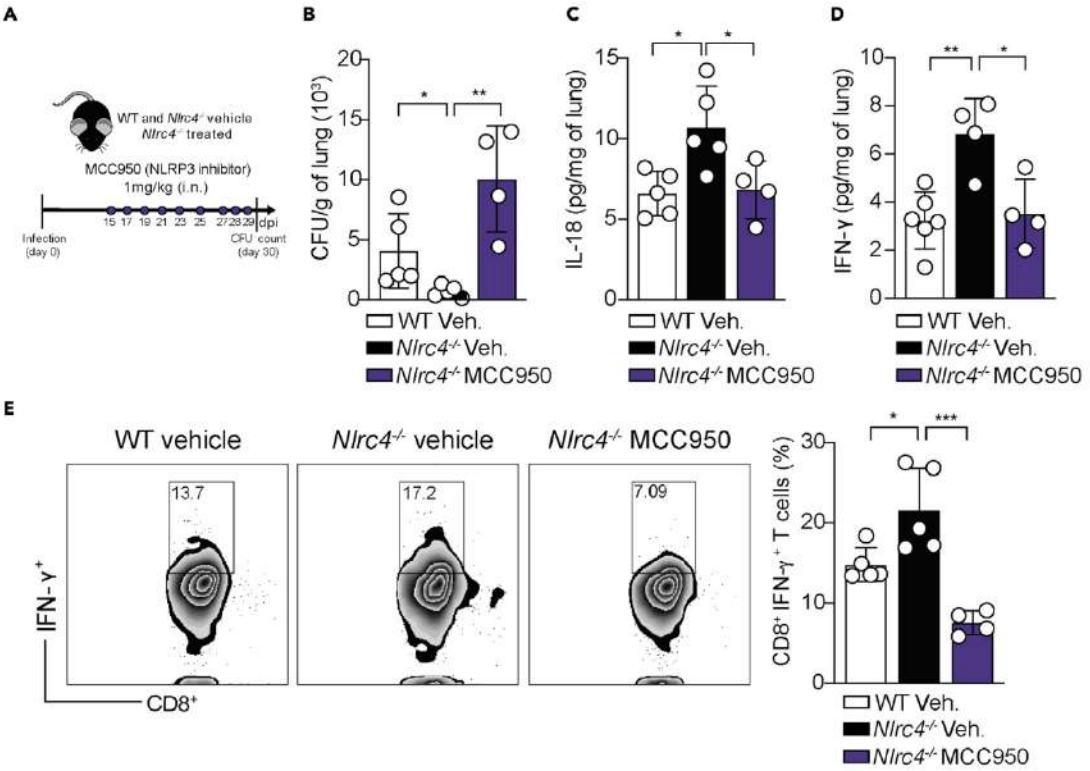

Figure 6. NLRC4 acts as a negative regulator of NLRP3 and affects protective Th1 responses in late stage of *P. brasiliensis* infection

WT and *Nlrc4*$^{-/-}$ mice were intravenously infected with 1x10^6 of viable Pb18 yeasts and the lungs were collected at 30 dpi.

(A) Schematic representation of the treatment with MCC950 (intranasal 1mg/kg).

(B) Scatterplots with bars show the CFU counting in lungs from WT and *Nlrc4*$^{-/-}$ mice treated or not with MCC950 (1 mg/kg) after 30 days of infection with 1x10^6 Pb18 yeasts.

(C and D) Scatterplots with bars show the quantification of IL-18 (C) and IFN-γ (D) by ELISA in the lungs at 30dpi.

(E) Contour plots represent flow cytometry data of CD8$^+$IFN-γ$^+$ T cells and scatterplots with bars show the percentage of CD8$^+$IFN-γ$^+$ T cells in the lungs. Data represent one independent experiment (n= 4-6 WT or *Nlrc4*$^{-/-}$ control mice and n = 4 *Nlrc4*$^{-/-}$ MCC950-treated mice per group). Data are expressed as mean ± SD. Statistically significant differences were evaluated with ANOVA followed by Bonferroni's multiple comparisons test (*p < 0.05, **p < 0.01, ***p < 0.001).

previously that both caspase-1 and caspase-8 synergize with NLRP3 inflammasome and contribute to IL-1β maturation and host resistance *in vivo* (Ketelut-Carneiro et al, 2015, 2018).

Interestingly, NLRC4 inflammasome activation in response to *Burkholderia pseudomallei* mediates pyroptosis, which is critical to control bacterial replication. In this study, the authors demonstrated that *Nlrc4*$^{-/-}$ mice produced higher amounts of IL-1β and IL-18 as a result of reduced cell death. While IL-1β mediated deleterious neutrophil influx to the lungs, IL-18 was required for protective IFN-γ production (Ceballos-Olvera et al., 2011). In our study, we observed significant accumulation of macrophages and DCs in the lungs of *Nlrc4*$^{-/-}$ mice, which accounted for higher IL-1β production. BMDMs from *Nlrc4*$^{-/-}$ mice also produced more IL-1β and NO and exhibited potent fungicidal activity against Pb18 *in vitro*. In concordance, fungal load was reduced in *Nlrc4*$^{-/-}$ mice at early stages of infection. It is possible that the earlier wave of IL-1β induces NOS2 expression and increases NO production in the lungs of *Nlrc4*$^{-/-}$ mice, partially controlling fungal replication until the development of a more effective CD8$^+$T cell-mediated IFN-γ response.

Studies with *A. fumigatus* have suggested that NLRC4 deficiency induces upregulation of NLRP3 expression and IL-1β production, which is associated with a lower fungal load at 14 dpi (Iannitti et al., 2016). Overall, our data indicate that NLRC4 modulates NLRP3-dependent IL-1β production, which is tightly correlated with expression of *Ptgs2* (COX-2) and PGE_2 production in the lungs of *Nlrc4*$^{-/-}$ mice. NLRP3 activation is

mediated by two signals: the priming that increases *Nlrp3* and *Il1b* transcription and the second signal that is triggered by pathogen-associated molecular patterns generated during microbial infection and endogenous danger signals (danger-associated molecular patterns) released from damaged or dying cells (Mariathasan and Monack, 2007). It has been shown that PGE_2 increases *Nlrp3* and *Il1b* transcription via EP2/4 receptor/cyclic adenosine monophosphate/protein kinase A/NF-κB pathway (Zoccal et al., 2016). Interestingly, we found that COX-2 inhibition and reduced PGE_2 production accounted for diminished IL-1β production and higher fungal burdens in *Nlrc4*$^{-/-}$ mice. The inhibition of COX-2 and selective inhibition of microsomal prostaglandin E synthase (mPTGES-1) in BMDMs revealed that the effect on PGE_2 production does not seem to be specific to *Nlrc4*$^{-/-}$ phenotype with IL-1β release and *Nlrp3* expression as a readout. Moreover, selective inhibition of mPTGES-1 only increased CFU counts in Pb18-infected *Nlrc4*$^{-/-}$ BMDMs, suggesting an additional role for PGE_2 in resistance to *P. brasiliensis* infection. The potent fungicidal activity of PGE_2 *in vitro* supports this hypothesis.

NLRP3 inflammasome activity promotes Th1/Th17 expansion during PCM (Feriotti et al., 2017). Interestingly, while IL-1β are equally expressed by WT and *Nlrc4*$^{-/-}$ mice at later stages of *P. brasiliensis* infection, sustained *Nlrp3* expression in this period of infection also enables higher IL-18 secretion. Consistently, our group has shown that NLRP3 activation mediates IL-18 secretion at 30 dpi (Ketelut-Carneiro et al., 2015), while caspase-11-mediated IL-1α release boosts adaptive Th17 responses (Ketelut-Carneiro et al., 2019). Nonetheless, our data demonstrate that NLRC4 impairs the activation of the NLRP3 inflammasome and production of IL-18 but does not change Th17-cytokine profile in the lungs of *Nlrc4*$^{-/-}$ mice at 30dpi.

IL-18 is critical for the development of effective Th1 response to the fungus (Ketelut-Carneiro et al., 2015; Mencacci et al., 2000; Stuyt et al., 2002). NLRC4 inflammasome has been linked to adaptative immune responses (Deets and Vance, 2021). Indeed, NLRC4 inflammasome impacts the development of $CD8^+$ T cell responses to bacterial infection (Theisen and Sauer, 2016). The recognition of flagellin by DCs induces IL-18 release after NLRC4 inflammasome activation to trigger IFN-γ production by memory $CD8^+$ T cells (Kupz et al., 2012). Furthermore, a recent study showed that NLRC4 negatively regulates NLRP3 activation, which impacts the secretion of IL-18 and IFN-γ during *Salmonella* infection (Tourlomousis et al., 2020). The increase of IL-18 levels in the lung from *P. brasiliensis*-infected *Nlrc4*$^{-/-}$ mice boosted Th1 cells responses, reflected by elevated levels of IFN-γ. This cytokine profile was accompanied by increased numbers of IFN-γ-producing $CD8^+$ T cells as well cytotoxic $CD8^+$ T cells (perforin$^+$ and granzyme-B$^+$). Either the absence of ASC or the pharmacological inhibition of NLRP3 inflammasome in NLRC4-deficient mice restrained IFN-γ production and reduced $CD8^+$ IFN-γ^+ T cells in the lungs. Corroborating the major role of this lymphocyte subset for resistance, $CD8^+$ T depletion, but not $CD4^+$ T cell and B cells, drives susceptibility to PCM (Chiarella et al., 2007).

In conclusion, this study demonstrates a pathogenic activity for NLRC4 during *P. brasiliensis* infection. NLRC4 affects NLRP3 inflammasome activity, suppressing early IL-1β-mediated fungicide mechanisms. At later stages of infection, reduced NLRP3 inflammasome activity limits IL-18 secretion and abrogates an effective antifungal $CD8^+$T cell-mediated IFN-γ response.

Limitations of the study

In the present study, we demonstrated that NLRC4 promotes susceptibility to experimental *P. brasiliensis* infection. Mechanistically, NLRC4 inhibits PGE_2 production, which is required for NLRP3-inflammasome-triggered IL-1β at the early phase of infection, while in the later phase of infection reduces IL-18 levels, abrogates $CD8^+$ IFN-γ^+ T cell responses, and promotes uncontrolled fungal growth. Although NLRC4 affects PGE_2 biosynthesis, its mechanism has to be investigated. It is possible that NLRC4 activation controls Ca^{2+}-dependent signaling (Iannitti et al., 2016; Wang et al., 2016), known to promote PGE_2 (Zoccal et al., 2016) and NLRP3 activation (Murakami et al., 2012). Of note, the difference of tissue colonization by pathogenic fungi is an important point to understand the specific role of NLRC4. Because we used total knockout mice, we were unable to reach a definitive conclusion on whether NLRC4 indeed operates at the hematopoietic compartment, such as macrophages and DCs or its activity on non-hematopoietic cells could actually be responsible for the reduced NLRP3 activity and susceptibility to infection *in vivo*. Importantly, the molecular mechanism by which NLRC4 inhibits NLRP3 inflammasome activity still needs to be elucidated. Future studies are required to understand how different NLR receptors interact with

each other to protect or promote infection, which could also reveal pathogenic roles of NLRC4 in other infections and diseases.

STAR★METHODS

Detailed methods are provided in the online version of this paper and include the following:

- KEY RESOURCES TABLE
- RESOURCE AVAILABILITY
  - Lead contact
  - Materials availability
  - Data and code availability
- EXPERIMENTAL MODEL AND SUBJECT DETAILS
  - Animals
  - Fungus and *in vivo* infection
- METHODS DETAILS
  - Bone-marrow-derived macrophages (BMDMs) and infection
  - Colony-forming units
  - Histopathological analyses
  - Immunohistochemistry
  - Cytokine detection
  - Western blotting
  - Quantitative real-time polymerase chain reaction
  - Killing assay and NO detection
  - Lung cell isolation and flow cytometry
  - Indomethacin treatment
  - PGE_2 quantification
  - MCC950 treatment
- QUANTIFICATION AND STATISTICAL ANALYSIS
  - Statistical analysis

SUPPLEMENTAL INFORMATION

Supplemental information can be found online at https://doi.org/10.1016/j.isci.2021.102548.

ACKNOWLEDGMENTS

We thank Denise Ferraz, Wander C. Ribeiro and Franciele Pioto for technical assistance. Júlio A. Siqueira, Rubilian C. Quineiro, Edinelson Mazzotto and Adriana Sestari for animal maintenance and all and Silva's laboratory members for their scientific discussions and insightful comments. We also thank Prof. Dr. Dario Zamboni and Prof. Dra. Daniela Carlos for providing animals and reagents. The research leading to these results was funded by the Fundação de Amparo à Pesquisa do Estado de São Paulo (FAPESP) under the grant agreement n° 2012/14524-9 (Thematic Project to J.S.S.) and 2013/08216-2 (Center for Research in Inflammatory Disease), from the University of São Paulo NAP-DIN under grant agreement n.° 11.1.21625.01.0. C.O.S.S. was supported by Master fellowships from FAPESP (grant n° 2015/21605-3) and Coordenação de Aperfeiçoamento de Pessoal de Nível Superior (CAPES). N.K.-C. was supported by doctoral and post-doctoral fellowships from FAPESP (grant n° 2013/21295-9) and Coordenação de Aperfeiçoamento de Pessoal de Nível Superior (CAPES), respectively. J.S.S. and L.H.F. are research fellows from Conselho Nacional de Desenvolvimento Científico e Tecnológico (CNPq).

AUTHOR CONTRIBUTIONS

C.O.S.S., N.K-C., and J.S.S. conceived the study. C.O.S.S., N.K-C., C.M., and L.G.G. performed experiments. C.O.O.S., N.K-C., and L.G.G. conducted data analysis. C.O.S.S. wrote the original draft. C.O.O.S., N.K-C., L.G.G., and J.S.S. reviewed and edited the article. C.O.S.S., N.K-C., L.H.F., L.G.G., and J.S.S. inputted intellectual concepts. J.S.S. provided resources and coordinated the study. All authors read and approved the final manuscript.

DECLARATION OF INTERESTS

The authors declare no competing interests.

Received: November 3, 2020
Revised: April 6, 2021
Accepted: May 14, 2021
Published: June 25, 2021

REFERENCES

Amer, A., Franchi, L., Kanneganti, T.-D., Body-Malapel, M., Ozören, N., Brady, G., Meshinchi, S., Jagirdar, R., Gewirtz, A., Akira, S., and Núñez, G. (2006). Regulation of Legionella phagosome maturation and infection through flagellin and host Ipaf. J. Biol. Chem. *281*, 35217–35223. https://doi.org/10.1074/jbc.M604933200.

Andrade, W.A., and Zamboni, D.S. (2020). NLRC4 biology in immunity and inflammation. J. Leukoc. Biol. *108*, 1117–1127. https://doi.org/10.1002/JLB.3MR0420-573R.

Balderramas, H.A., Penitenti, M., Rodrigues, D.R., Bachiega, T.F., Fernandes, R.K., Ikoma, M.R.V., Dias-Melicio, L.A., Oliveira, S.L., and Soares, Â.M.V.C. (2014). Human neutrophils produce IL-12, IL-10, PGE2 and LTB4 in response to Paracoccidioides brasiliensis. Involvement of TLR2, mannose receptor and dectin-1. Cytokine *67*, 36–43. https://doi.org/10.1016/j.cyto.2014.02.004.

Bauernfeind, F., and Hornung, V. (2013). Of inflammasomes and pathogens – sensing of microbes by the inflammasome. EMBO Mol. Med. *5*, 814–826. https://doi.org/10.1002/emmm.201201771.

Bordon, A.P., Dias-Melicio, L.A., Acorci, M.J., Biondo, G.A., Fecchio, D., Peraçoli, M.T.S., and de Soares, A.M.V.C. (2007). Prostaglandin E(2) production by high and low virulent strains of Paracoccidioides brasiliensis. Mycopathologia *163*, 129–135. https://doi.org/10.1007/s11046-007-0098-1.

Borghi, M., De Luca, A., Puccetti, M., Jaeger, M., Mencacci, A., Oikonomou, V., Pariano, M., Garlanda, C., Moretti, S., Bartoli, A., et al. (2015). Pathogenic NLRP3 inflammasome activity during Candida infection is negatively regulated by IL-22 via activation of NLRC4 and IL-1Ra. Cell Host Microbe *18*, 198–209. https://doi.org/10.1016/j.chom.2015.07.004.

Brummer, E., Hanson, L.H., Restrepo, A., and Stevens, D.A. (1988). In vivo and in vitro activation of pulmonary macrophages by IFN-gamma for enhanced killing of Paracoccidioides brasiliensis or Blastomyces dermatitidis. J. Immunol. *140*, 2786–2789.

Calich, V.L., Vaz, C.A., and Burger, E. (1998). Immunity to Paracoccidioides brasiliensis infection. Res. Immunol. *149*, 407–417, discussion 499-500.

Ceballos-Olvera, I., Sahoo, M., Miller, M.A., Del Barrio, L., and Re, F. (2011). Inflammasome-dependent pyroptosis and IL-18 protect against Burkholderia pseudomallei lung infection while IL-1β is deleterious. PLoS Pathog. *7*, e1002452. https://doi.org/10.1371/journal.ppat.1002452.

Chiarella, A.P., Arruda, C., Pina, A., Costa, T.A., Ferreira, R.C.V., and Calich, V.L.G. (2007). The relative importance of CD4+ and CD8+T cells in immunity to pulmonary paracoccidioidomycosis. Microbes Infect. *9*, 1078–1088. https://doi.org/10.1016/j.micinf.2007.04.016.

Deets, K.A., and Vance, R.E. (2021). Inflammasomes and adaptive immune responses. Nat. Immunol. *22*, 412–422. https://doi.org/10.1038/s41590-021-00869-6.

Feriotti, C., de Araújo, E.F., Loures, F.V., da Costa, T.A., Galdino, N.A.de L., Zamboni, D.S., and Calich, V.L.G. (2017). NOD-like receptor P3 inflammasome controls protective Th1/Th17 immunity against pulmonary paracoccidioidomycosis. Front. Immunol. *8*, 786. https://doi.org/10.3389/fimmu.2017.00786.

Figueiredo, F., Alves, L.M., and Silva, C.L. (1993). Tumour necrosis factor production in vivo and in vitro in response to Paracoccidioides brasiliensis and the cell wall fractions thereof. Clin. Exp. Immunol. *93*, 189–194. https://doi.org/10.1111/j.1365-2249.1993.tb07964.x.

Franco, M. (1987). Host-parasite relationships in paracoccidioidomycosis. J. Med. Vet. Mycol. Bimon. Publ. Int. Soc. Hum. Anim. Mycol. *25*, 5–18.

Gonzalez, A., Gregori, W.de, Velez, D., Restrepo, A., and Cano, L.E. (2000). Nitric oxide participation in the fungicidal mechanism of gamma interferon-activated murine macrophages againstParacoccidioides brasiliensis conidia. Infect. Immun. *68*, 2546–2552. https://doi.org/10.1128/IAI.68.5.2546-2552.2000.

He, Y., Hara, H., and Núñez, G. (2016). Mechanism and regulation of NLRP3 inflammasome activation. Trends Biochem. Sci. *41*, 1012–1021. https://doi.org/10.1016/j.tibs.2016.09.002.

Hua, K.-F., Chou, J.-C., Ka, S.-M., Tasi, Y.-L., Chen, A., Wu, S.-H., Chiu, H.-W., Wong, W.-T., Wang, Y.-F., Tsai, C.-L., et al. (2015). Cyclooxygenase-2 regulates NLRP3 inflammasome-derived IL-1β production. J. Cell. Physiol. *230*, 863–874. https://doi.org/10.1002/jcp.24815.

Iannitti, R.G., Napolioni, V., Oikonomou, V., De Luca, A., Galosi, C., Pariano, M., Massi-Benedetti, C., Borghi, M., Puccetti, M., Lucidi, V., et al. (2016). IL-1 receptor antagonist ameliorates inflammasome-dependent inflammation in murine and human cystic fibrosis. Nat. Commun. *7*, 10791. https://doi.org/10.1038/ncomms10791.

Joly, S., Ma, N., Sadler, J.J., Soll, D.R., Cassel, S.L., and Sutterwala, F.S. (2009). Cutting edge: Candida albicans hyphae formation triggers activation of the Nlrp3 inflammasome. J. Immunol. *183*, 3578–3581. https://doi.org/10.4049/jimmunol.0901323.

Ketelut-Carneiro, N., and Fitzgerald, K.A. (2020). Inflammasomes. Curr. Biol. *30*, R689–R694. https://doi.org/10.1016/j.cub.2020.04.065.

Ketelut-Carneiro, N., Ghosh, S., Levitz, S.M., Fitzgerald, K.A., and da Silva, J.S. (2018). A dectin-1-caspase-8 pathway licenses canonical caspase-1 inflammasome activation and interleukin-1β release in response to a pathogenic fungus. J. Infect. Dis. *217*, 329–339. https://doi.org/10.1093/infdis/jix568.

Ketelut-Carneiro, N., Silva, G.K., Rocha, F.A., Milanezi, C.M., Cavalcanti-Neto, F.F., Zamboni, D.S., and Silva, J.S. (2015). IL-18 triggered by the Nlrp3 inflammasome induces host innate resistance in a pulmonary model of fungal infection. J. Immunol. *194*, 4507–4517. https://doi.org/10.4049/jimmunol.1402321.

Ketelut-Carneiro, N., Souza, C.O.S., Benevides, L., Gardinassi, L.G., Silva, M.C., Tavares, L.A., Zamboni, D.S., and Silva, J.S. (2019). Caspase-11-dependent IL-1α release boosts Th17 immunity against Paracoccidioides brasiliensis. PLoS Pathog. *15*, e1007990. https://doi.org/10.1371/journal.ppat.1007990.

Kupz, A., Guarda, G., Gebhardt, T., Sander, L.E., Short, K.R., Diavatopoulos, D.A., Wijburg, O.L.C., Cao, H., Waithman, J.C., Chen, W., et al. (2012). NLRC4 inflammasomes in dendritic cells regulate noncognate effector function by memory $CD8^+$ T cells. Nat. Immunol. *13*, 162–169. https://doi.org/10.1038/ni.2195.

Kurita, N., Oarada, M., and Brummer, E. (2005). Fungicidal activity of human peripheral blood leukocytes against Paracoccidioides brasiliensis yeast cells. Med. Mycol. *43*, 417–422. https://doi.org/10.1080/13693780400011088.

Lara-Tejero, M., Sutterwala, F.S., Ogura, Y., Grant, E.P., Bertin, J., Coyle, A.J., Flavell, R.A., and Galán, J.E. (2006). Role of the caspase-1 inflammasome in Salmonella typhimurium pathogenesis. J. Exp. Med. *203*, 1407–1412. https://doi.org/10.1084/jem.20060206.

Lima-Junior, D.S., Costa, D.L., Carregaro, V., Cunha, L.D., Silva, A.L.N., Mineo, T.W.P., Gutierrez, F.R.S., Bellio, M., Bortoluci, K.R., Flavell, R.A., et al. (2013). Inflammasome-derived IL-1β production induces nitric oxide-mediated resistance to Leishmania. Nat. Med. *19*, 909–915. https://doi.org/10.1038/nm.3221.

Mariathasan, S., and Monack, D.M. (2007). Inflammasome adaptors and sensors: intracellular regulators of infection and inflammation. Nat. Rev. Immunol. *7*, 31–40. https://doi.org/10.1038/nri1997.

Mariathasan, S., Newton, K., Monack, D.M., Vucic, D., French, D.M., Lee, W.P., Roose-Girma, M., Erickson, S., and Dixit, V.M. (2004). Differential activation of the inflammasome by caspase-1 adaptors ASC and Ipaf. Nature *430*, 213–218. https://doi.org/10.1038/nature02664.

Mariathasan, S., Weiss, D.S., Newton, K., McBride, J., O'Rourke, K., Roose-Girma, M., Lee, W.P., Weinrauch, Y., Monack, D.M., and Dixit, V.M. (2006). Cryopyrin activates the inflammasome in response to toxins and ATP.

Nature *440*, 228–232. https://doi.org/10.1038/nature04515.

Marim, F.M., Silveira, T.N., Lima, D.S., and Zamboni, D.S. (2010). A method for generation of bone marrow-derived macrophages from cryopreserved mouse bone marrow cells. PLoS One *5*, e15263. https://doi.org/10.1371/journal.pone.0015263.

Martinez, R. (2017). New trends in paracoccidioidomycosis epidemiology. J. Fungi *3*, 1. https://doi.org/10.3390/jof3010001.

Martinon, F., Burns, K., and Tschopp, J. (2002). The inflammasome: a molecular platform triggering activation of inflammatory caspases and processing of proIL-beta. Mol. Cell *10*, 417–426. https://doi.org/10.1016/s1097-2765(02)00599-3.

Mencacci, A., Bacci, A., Cenci, E., Montagnoli, C., Fiorucci, S., Casagrande, A., Flavell, R.A., Bistoni, F., and Romani, L. (2000). Interleukin 18 restores defective Th1 immunity to Candida albicans in caspase 1-deficient mice. Infect. Immun. *68*, 5126–5131.

Miao, E.A., Mao, D.P., Yudkovsky, N., Bonneau, R., Lorang, C.G., Warren, S.E., Leaf, I.A., and Aderem, A. (2010). Innate immune detection of the type III secretion apparatus through the NLRC4 inflammasome. Proc. Natl. Acad. Sci. U S A *107*, 3076–3080. https://doi.org/10.1073/pnas.0913087107.

Michelin, M.A., Figueiredo, F., and Cunha, F.Q. (2002). Involvement of prostaglandins in the immunosuppression occurring during experimental infection by Paracoccidioides brasiliensis. Exp. Parasitol. *102*, 170–177.

Murakami, T., Ockinger, J., Yu, J., Byles, V., McColl, A., Hofer, A.M., and Horng, T. (2012). Critical role for calcium mobilization in activation of the NLRP3 inflammasome. Proc. Natl. Acad. Sci. *109*, 11282–11287. https://doi.org/10.1073/pnas.1117765109.

Pedraza-Alva, G., Pérez-Martínez, L., Valdez-Hernández, L., Meza-Sosa, K.F., and Ando-Kuri, M. (2015). Negative regulation of the inflammasome: keeping inflammation under control. Immunol. Rev. *265*, 231–257. https://doi.org/10.1111/imr.12294.

Plato, A., Hardison, S.E., and Brown, G.D. (2015). Pattern recognition receptors in antifungal immunity. Semin. Immunopathol. *37*, 97–106. https://doi.org/10.1007/s00281-014-0462-4.

Rauch, I., Deets, K.A., Ji, D.X., von Moltke, J., Tenthorey, J.L., Lee, A.Y., Philip, N.H., Ayres, J.S., Brodsky, I.E., Gronert, K., and Vance, R.E. (2017). NAIP-NLRC4 inflammasomes coordinate intestinal epithelial cell expulsion with eicosanoid and IL-18 release via activation of caspase-1 and -8. Immunity *46*, 649–659. https://doi.org/10.1016/j.immuni.2017.03.016.

Schneider, C.A., Rasband, W.S., and Eliceiri, K.W. (2012). NIH Image to ImageJ: 25 years of image analysis. Nat. Methods *9*, 671–675. https://doi.org/10.1038/nmeth.2089.

Sokolowska, M., Chen, L.-Y., Liu, Y., Martinez-Anton, A., Qi, H.-Y., Logun, C., Alsaaty, S., Park, Y.H., Kastner, D.L., Chae, J.J., and Shelhamer, J.H. (2015). Prostaglandin E2 inhibits NLRP3 inflammasome activation through EP4 receptor and intracellular cyclic AMP in human macrophages. J. Immunol. *194*, 5472–5487. https://doi.org/10.4049/jimmunol.1401343.

Sorgi, C.A., Zarini, S., Martin, S.A., Sanchez, R.L., Scandiuzzi, R.F., Gijón, M.A., Guijas, C., Flamand, N., Murphy, R.C., and Faccioli, L.H. (2017). Dormant 5-lipoxygenase in inflammatory macrophages is triggered by exogenous arachidonic acid. Sci. Rep. *7*, 10981. https://doi.org/10.1038/s41598-017-11496-3.

Souza, C.O.S., Espíndola, M.S., Fontanari, C., Prado, M.K.B., Frantz, F.G., Rodrigues, V., Gardinassi, L.G., and Faccioli, L.H. (2018). CD18 regulates monocyte hematopoiesis and promotes resistance to experimental schistosomiasis. Front. Immunol. *9*, 1970. https://doi.org/10.3389/fimmu.2018.01970.

Stuyt, R.J.L., Netea, M.G., Verschueren, I., Fantuzzi, G., Dinarello, C.A., Van der Meer, J.W.M., and Kullberg, B.J. (2002). Role of interleukin-18 in host defense against disseminated Candida albicans infection. Infect. Immun. *70*, 3284–3286. https://doi.org/10.1128/IAI.70.6.3284-3286.2002.

Sutterwala, F.S., Mijares, L.A., Li, L., Ogura, Y., Kazmierczak, B.I., and Flavell, R.A. (2007). Immune recognition of Pseudomonas aeruginosa mediated by the IPAF/NLRC4 inflammasome. J. Exp. Med. *204*, 3235–3245. https://doi.org/10.1084/jem.20071239.

Sutterwala, F.S., Ogura, Y., Szczepanik, M., Lara-Tejero, M., Lichtenberger, G.S., Grant, E.P., Bertin, J., Coyle, A.J., Galán, J.E., Askenase, P.W., and Flavell, R.A. (2006). Critical role for NALP3/CIAS1/Cryopyrin in innate and adaptive immunity through its regulation of caspase-1. Immunity *24*, 317–327. https://doi.org/10.1016/j.immuni.2006.02.004.

Suzuki, T., Franchi, L., Toma, C., Ashida, H., Ogawa, M., Yoshikawa, Y., Mimuro, H., Inohara, N., Sasakawa, C., and Nuñez, G. (2007). Differential regulation of caspase-1 activation, pyroptosis, and autophagy via ipaf and ASC in shigella-infected macrophages. PLoS Pathog. *3*, e111. https://doi.org/10.1371/journal.ppat.0030111.

Tang, T., Gong, T., Jiang, W., and Zhou, R. (2018). GPCRs in NLRP3 inflammasome activation, regulation, and therapeutics. Trends Pharmacol. Sci. *39*, 798–811. https://doi.org/10.1016/j.tips.2018.07.002.

Tate, M.D., Ong, J.D.H., Dowling, J.K., McAuley, J.L., Robertson, A.B., Latz, E., Drummond, G.R., Cooper, M.A., Hertzog, P.J., and Mansell, A. (2016). Reassessing the role of the NLRP3 inflammasome during pathogenic influenza A virus infection via temporal inhibition. Sci. Rep. *6*, 27912. https://doi.org/10.1038/srep27912.

Tavares, A.H., Bürgel, P.H., and Bocca, A.L. (2015). Turning up the heat: inflammasome activation by fungal pathogens. PLoS Pathog. *11*, e1004948. https://doi.org/10.1371/journal.ppat.1004948.

Tavares, A.H., Magalhães, K.G., Almeida, R.D.N., Correa, R., Burgel, P.H., and Bocca, A.L. (2013). NLRP3 inflammasome activation by Paracoccidioides brasiliensis. PLoS Negl. Trop. Dis. *7*, e2595. https://doi.org/10.1371/journal.pntd.0002595.

Theisen, E., and Sauer, J.-D. (2016). Listeria monocytogenes-induced cell death inhibits the generation of cell-mediated immunity. Infect. Immun. *85*. https://doi.org/10.1128/IAI.00733-16.

Tomalka, J., Ganesan, S., Azodi, E., Patel, K., Majmudar, P., Hall, B.A., Fitzgerald, K.A., and Hise, A.G. (2011). A novel role for the NLRC4 inflammasome in mucosal defenses against the fungal pathogen Candida albicans. PLoS Pathog. *7*, e1002379. https://doi.org/10.1371/journal.ppat.1002379.

Tourlomousis, P., Wright, J.A., Bittante, A.S., Hopkins, L.J., Webster, S.J., Bryant, O.J., Mastroeni, P., Maskell, D.J., and Bryant, C.E. (2020). Modifying bacterial flagellin to evade Nod-like Receptor CARD 4 recognition enhances protective immunity against Salmonella. Nat. Microbiol. *5*, 1588–1597. https://doi.org/10.1038/s41564-020-00801-y.

Tristão, F.S.M., Rocha, F.A., Carlos, D., Ketelut-Carneiro, N., Souza, C.O.S., Milanezi, C.M., and Silva, J.S. (2017). Th17-Inducing cytokines IL-6 and IL-23 are crucial for granuloma formation during experimental paracoccidioidomycosis. Front. Immunol. *8*, 949. https://doi.org/10.3389/fimmu.2017.00949.

Tristão, F.S.M., Rocha, F.A., Dias, F.C., Rossi, M.A., and Silva, J.S. (2013). The left lung is preferentially targeted during experimental paracoccidioidomycosis in C57BL/6 mice. Braz. J. Med. Biol. Res. *46*, 839–843. https://doi.org/10.1590/1414-431X20133140.

von Moltke, J., Trinidad, N.J., Moayeri, M., Kintzer, A.F., Wang, S.B., van Rooijen, N., Brown, C.R., Krantz, B.A., Leppla, S.H., Gronert, K., and Vance, R.E. (2012). Rapid induction of inflammatory lipid mediators by the inflammasome in vivo. Nature *490*, 107–111. https://doi.org/10.1038/nature11351.

Wang, X., Shaw, D.K., Hammond, H.L., Sutterwala, F.S., Rayamajhi, M., Shirey, K.A., Perkins, D.J., Bonventre, J.V., Velayutham, T.S., Evans, S.M., et al. (2016). The prostaglandin E2-EP3 receptor Axis regulates Anaplasma phagocytophilum-mediated NLRC4 inflammasome activation. PLoS Pathog. *12*, e1005803. https://doi.org/10.1371/journal.ppat.1005803.

Zoccal, K.F., Sorgi, C.A., Hori, J.I., Paula-Silva, F.W.G., Arantes, E.C., Serezani, C.H., Zamboni, D.S., and Faccioli, L.H. (2016). Opposing roles of LTB 4 and PGE 2 in regulating the inflammasome-dependent scorpion venom-induced mortality. Nat. Commun. *7*, 10760. https://doi.org/10.1038/ncomms10760.

STAR★METHODS

KEY RESOURCES TABLE

REAGENT or RESOURCE	SOURCE	IDENTIFIER
Antibodies		
FITC anti-mouse CD3ε (clone: 145-2C11)	BioLegend	Cat#100306; RRID:AB_312671
Pacific Blue™ anti-mouse CD4 (clone: RM4-4)	BioLegend	Cat#116008; RRID:AB_11149680
PE-Cy7™ or PerCP anti-mouse CD8a (clone: 53-6.7)	BD Bioscience	Cat#552877; RRID:AB_394506 or Cat#553036; RRID:AB_394573
Pacific Blue™ anti-mouse CD45 (clone: 30-F11)	BioLegend	Cat#103126; RRID:AB_493535
PE anti-human/mouse CD11b (clone: M1/70)	BioLegend	Cat#101208; RRID:AB_312791
PE/Cyanine7 anti-mouse CD11c (clone: N418)	BioLegend	Cat#117318; RRID:AB_493568
FITC anti-mouse I-A/I-E (clone: M5/114.5.2)	BD Bioscience	Cat#553623; RRID:AB_394958
PerCP anti-mouse Ly6C (clone: HK1.4)	BioLegend	Cat#128028; RRID:AB_10897805
Alexa Fluor® 488 anti-mouse Ly6G (clone:1A8)	BioLegend	Cat#127626; RRID:AB_2561340
APC anti-mouse IFN-γ (clone: XM 61.2)	BioLegend	Cat#505810; RRID:AB_315404
APC anti-human/mouse IL-1β (pro-form) (clone: NJTEN3)	eBioscience	Cat#17-7114-80; RRID:AB_10670739
PE anti-mouse Perforin (clone: eBioOMAK-D)	eBioscience	Cat#12-9392-82; RRID:AB_466242
Alexa Flour® 647 anti-human/mouse Granzyme B (clone:GB11)	BioLegend	Cat#515405; RRID:AB_2294995
PE anti-mouse Granzyme A (clone: 3G8.5)	BioLegend	Cat#149704; RRID:AB_2565310
Rabbit polyclonal to IL-1β	Abcam	Cat#ab9722; RRID:AB_308765
Goat polyclonal anti-Caspase-1 p20	Santa Cruz Biotechnology	Cat#sc-1597; RRID:AB_2068887
Rabbit polyclonal NOS2	Santa Cruz Biotechnology	Cat#sc-650; RRID:AB_631831
Rat monoclonal anti-Caspase-1 p20	Genentech	Clone:4B4
Goat polyclonal anti-IL-1β	Sigma-Aldrich	Cat#I3767-1MG; RRID:AB_477105
Rabbit mAb cleaved Caspase-8 (Asp387) (D5B2) XP®	Cell Signaling Technology	Cat#8592S; RRID:AB_10891784
Rabbit polyclonal anti-beta Actin	Abcam	Cat#ab8227; RRID:AB_2305186
*InVivo*MAb anti-mouse/rat IL-1β (clone:B122)	BioXCell	Cat#BE0246; RRID:AB_2687727
Chemicals, peptides, and recombinant proteins		
Recombinant mouse IFN-γ	Biolegend	Cat#575304
Recombinant mouse IL-1β/IL-1F2 Protein	R&D Systems	Cat#401-ML
MCC950	InvivoGen	Cat#inh-mcc
Aminoguanidine hydrochloride	Sigma-Aldrich	Cat#19371-19-5
PGE_2	Cayman Chemical	Cat#14010
CAY10526	Cayman Chemical	Cat#10010088
Indomethacin	Sigma-Aldrich	Cat#I8280
Nigericin sodium salt	Sigma-Aldrich	Cat#N7143
LPS-EK Ultrapure	InvivoGen	Cat#tlrl-peklps
PMA	Abcam	Cat#ab120297
Ionomicina	Sigma-Aldrich	Cat#I0634
Brefeldin A	BioLegend	Cat#420601

(*Continued on next page*)

Continued

REAGENT or RESOURCE	SOURCE	IDENTIFIER
Deoxyribonuclease I from bovine pancreas	Sigma-Aldrich	Cat#DN25
Collagenase from *Clostridium histolyticum* (type IV)	Sigma-Aldrich	Cat#C5138
Critical commercial assays		
Mouse IL-1β ELISA MAX™ Standard Set	BioLegend	Cat#432601
Mouse TNF-α DuoSet ELISA	R&D Systems	Cat#DY410
Mouse IL-12/IL-23 (p40) ELISA MAX™ Standard Set	BioLegend	Cat#431603
Mouse IL-18 ELISA Kit	MBL	Cat#7625
Mouse IFN-γ ELISA MAX™ Standard Set	BioLegend	Cat#430801
Mouse IL-10 ELISA MAX™ Standard Set	BioLegend	Cat#431411
Mouse IL-1ra/IL-1F3 DuoSet ELISA	R&D Systems	Cat#DY480
Mouse IL-17 DuoSet ELISA	R&D Systems	Cat#DY421
Mouse IL-6 DuoSet ELISA	R&D Systems	Cat#DY406
Mouse CXCL1/KC DuoSet ELISA	R&D Systems	Cat#DY453
Mouse CXCL2/MIP-2 DuoSet ELISA	R&D Systems	Cat#DY452
Pierce™ Coomassie (Bradford) Protein Assay	Thermo Fisher Scientific	Cat#23200
Experimental models: Cell lines		
L-929	ATCC	ATCC CCL-1
Experimental models: Organisms/strains		
C57BL/6J mice	Jackson Laboratory	000664
NLRP3 knockout mice	Mariathasan et al., 2006	N/A
NLRC4 knockout mice	Lara-Tejero et al., 2006	N/A
ASC knockout mice	Sutterwala et al., 2006	N/A
NLRC4 and ASC double-knockout mice (*Nlrc4*$^{-/-}$*Asc*$^{-/-}$)	This paper	N/A
Paracoccidioides brasiliensis Pb18 strain	Figueiredo et al. (1993)	N/A
Oligonucleotides		
Mouse *Beta-2 microglobulin* forward	Ketelut-Carneiro et al. (2019)	5′ – CAC CCC CAC TGA GAC TGA TAC ATA – 3′
Mouse *Beta-2 microglobulin* reverse	Ketelut-Carneiro et al. (2019)	3′- TCA CAT GTC TCG ATC CCA GTA GA-5′
Mouse *Nlrp3* forward	This article	5′ – GCA GCG CAT CGC CTT CTA TC– 3′
Mouse *Nlrp3* reverse	This article	3′-CGG TGG TTG CTA GGA GAT GG-5′
Mouse *Ptgs2* forward	This article	5′ – GTG GAA AAA CCT CGT CCA GA– 3′
Mouse *Ptgs2* reverse	This article	3′- GCT CGG CTT CCA GTA TTG AG-5′
Mouse *iNos* forward	Ketelut-Carneiro et al. (2019)	5′ CGA AAC GCT TCA CTT CCA A 3′
Mouse *iNos* reverse	Ketelut-Carneiro et al. (2019)	3′ – TGA GCC TAT ATT GCT GTG GCT-5′
Software and algorithms		
Image J (v1.51)	Schneider et al. (2012)	https://imagej.nih.gov/ij/
GraphPad Prism 8.0	GraphPad Software	https://www.graphpad.com/scientific-software/prism/
FlowJo software (v10.0.7)	Tree Star, Inc, Ashland, OR, USA	https://www.flowjo.com/solutions/flowjo/downloads

(*Continued on next page*)

Continued

REAGENT or RESOURCE	SOURCE	IDENTIFIER
FACSDiva software (v8.0.1)	BD Biosciences	https://www.bdbiosciences.com/en-us/instruments/research-instruments/research-software/flow-cytometry-acquisition/facsdiva-software
Other		
iBright™ CL1500 Imaging System	Thermo Fisher Scientific	Cat#A44114
BD FACS CANTO™ II Cell Analyzer	BD Bioscience	https://www.bdbiosciences.com/en-us/instruments/research-instruments/research-cell-analyzers/facscanto-ii
TriploTOF® 5600+System	Sciex	https://sciex.com/br/products/mass-spectrometers/qtof-systems/tripletof-systems/tripletof-5600-system

RESOURCE AVAILABILITY

Lead contact

Further information and requests for resources and reagents should be directed to and will be fulfilled by the lead contact, João S. Silva (jsdsilva@fmrp.usp.br).

Materials availability

This study did not generate new materials or reagents.

Data and code availability

Data codes/sets were not generated or analyzed in this study. For questions regarding the raw data from the current study, please contact the corresponding author. All software's used in this study are commercially available.

EXPERIMENTAL MODEL AND SUBJECT DETAILS

Animals

Male 6- to 8-week-old C57BL/6 (WT) (Jackson Laboratory, stock number 000664) and *Nlrc4*$^{-/-}$ (Lara-Tejero et al., 2006), *Nlrp3*$^{-/-}$ (Mariathasan et al., 2006) and *Asc*$^{-/-}$ (Sutterwala et al., 2006) mice were obtained from the Isogenic Breeding Unit at Ribeirão Preto Medical School, USP, Brazil. All mice used in this study were in C57BL/6 genetic background. To obtain the *Nlrc4*$^{-/-}$*Asc*$^{-/-}$ mice (double Knockout mice), *Nlrc4*$^{-/-}$ and *Asc*$^{-/-}$ knockout mice were backcrossed. All mice were maintained under specific-pathogen-free conditions and provided food and water ad libitum, at 25°C. All experiments were approved and carried out in accordance with the Animal Ethics Committee from Ribeirão Preto Medical School (protocol no.046/2015).

Fungus and *in vivo* infection

Yeast cells of *P. brasiliensis* strain (Pb18) were cultured for 7 days at 36°C in Brain Heart Infusion (BHI) agar medium supplemented with 5% fetal bovine serum (FBS) and gentamicin (100 ng/mL), as described elsewhere (Figueiredo et al., 1993). To prepare the inoculum, yeasts were harvested and grown overnight under agitation in F12 Coon's Modification medium at 37°C. For *in vivo* infection, yeast cells were adjusted to $1x10^6$ in 100 µL of PBS and inoculated intravenously. At 7, 15, and 30 days post infection (dpi), mice were euthanized for collection of organs. Survival rates were monitored for 200 days.

METHODS DETAILS

Bone-marrow-derived macrophages (BMDMs) and infection

BMDMs were generated as previously described (Marim et al., 2010). Briefly, bone marrow cells were cultured for 7 days in RPMI supplemented with 30% L929 cell-conditioned medium and 20% FBS. BMDMs were infected with fungi at a multiplicity of infection (MOI) of 1 or 5. BMDMs primed with 500ng/mL ultrapure LPS (InvivoGen, tlrl-peklps) for 4 h and 20µM nigericin (Sigma-Aldrich) for 40 min were used as a positive control for inflammasome activation.

Colony-forming units

Viable yeasts in organs from Pb18-infected mice were determined by colony-forming unit (CFU) counting. BHI plates were incubated at 37°C for 7–14 days, and the amount of CFU per gram of tissue was calculated.

Histopathological analyses

Animals were randomly selected from each group at 30 dpi. Lung tissue was fixed with 10% formalin for 24 h and embedded in paraffin. Sections of 5μm were stained with hematoxylin and eosin (H&E) to evaluate inflammation, impregnated with silver for fungal cell labeling (Grocott method), or stained with picrosirus red to evaluate collagen deposition. Quantification of H&E and picrosirus stained images were estimated with ImageJ software (V1.51) (Schneider et al., 2012).

Immunohistochemistry

Lung sections (5μm) obtained at 7 dpi were incubated with primary antibodies to IL-1β (1:250; abcam 9722), caspase-1 (1:250; sc-1597) and nos2 (1:400; sc-650) diluted in PBS 0.01% saponin. Slides were counterstained with Mayer's hematoxylin counterstaining (Millipore, USA). Quantification of IL-1β, caspase-1, and NOS2 stained images were estimated with ImageJ software (V1.51) (Schneider et al., 2012).

Cytokine detection

Supernatants of BMDMs and lung-tissue homogenates were used to quantify the levels of IL-1β, IL-1Ra, TNF-α, IFN-γ, IL-6, IL-17, IL-10, IL-12p40, CXCL-1, CXCL-2 with ELISA kits from BioLegend and R&D Systems, and IL-18 with ELISA kit from MBL®,Woburn, MA.

Western blotting

For *in vivo*, the lungs were removed and homogenized in RIPA buffer (Sigma-Aldrich/Merck, Darmstadt, Germany) containing proteases inhibitor cocktail (Roche, Basel, Switzerland). Protein was quantified by Bradford assay (Pierce™ Coomassie [Bradford] Protein Assay) (Thermo Fisher Scientific, Waltham, MA, EUA). The supernatants were suspended with LDS Sample Buffer (4x) (Life Technologies). For *in vitro*, BMDM supernatants were denatured in loading buffer containing RIPA buffer, protease inhibitor, and LDS sample buffer (4x). Next, all samples were boiled and subjected to 4–12% SDS-polyacrylamide gel electrophoresis (PAGE) gel. The SDS-PAGE-separated proteins, transferred to nitrocellulose membranes, were immunoblotted with primary antibodies IL-1β (1:500; Sigma-Aldrich, St. Louis, MO, USA), caspase 1 p20 (1:500; clone 4B4, Genentech, San Francisco, CA, USA), caspase 8 (1:1000; cell singling #8592), and beta actin (1:5000; ab8227). Specific secondary antibodies were used afterward. Proteins in the blots were visualized by enhanced chemiluminescence using ECL (GE Healthcare). The data acquisition and bands were densitometrically quantified using iBright™ CL1500 Imaging System (Thermo Fisher Scientific, Waltham, MA, EUA) or ImageJ software (V1.51) (Schneider et al., 2012), and the results were expressed as arbitrary units.

Quantitative real-time polymerase chain reaction

Total RNA was extracted from lung homogenates or BMDM lysates using the TRIzol reagent (Life Technologies) and the SV Total RNA Isolation System Kit (Promega®) as per the manufacturer's instructions. Complementary DNA was synthesized with the High Capacity cDNA Reverse Transcription Kit (Applied Biosystems). SYBR-Green-Mix-based real-time quantitative polymerase chain reaction (PCR) assays were performed using the StepOnePlus Real-Time PCR System (Applied Biosystems). The mean cycle threshold (Ct) values of triplicate measurements were used to calculate the expression of the target genes, which were normalized to the housekeeping gene *β2m* and analyzed with the $2^{-\Delta\Delta Ct}$ method. Thus, were used for the quantitative PCR with the following primers: mouse Beta-2 microglobulin forward 5'-CAC CCC CAC TGA GAC TGA TAC ATA-3' and reverse 3'-TCA CAT GTC TCG ATC CCA GTA GA-5' ; mouse *Nlrp3* forward 5'-GCA GCG CAT CGC CTT CTA TC-3' and reverse 3'-CGG TGG TTG CTA GGA GAT GG-5'; mouse *Ptgs2* forward 5'-GTG GAA AAA CCT CGT CCA GA-3' and reverse 3'-GCT CGG CTT CCA GTA TTG AG-5'; mouse *iNos* forward 5'-CGA AAC GCT TCA CTT CCA A-3' and reverse 3'-TGA GCC TAT ATT GCT GTG GCT-5'. All primers were designed using the Primer Express software package v2.0 (Applied Biosystems), based on the nucleotide reference sequences available at GenBank database.

Killing assay and NO detection

The killing activity was adapted from (Kurita et al., 2005). Briefly, BMDMs were pretreated overnight with 50 ng/mL of recombinant IFN-γ (rIFN-γ; BioLegend), 20 ng/mL of recombinant IL-1β (rIL-1β ; RD 401-ML), 20 ng/mL of α-IL-1β (BioXCell; clone B122), 1mM of aminoguanidine (Sigma-Aldrich, St. Louis, MO, USA) or 30 min before with 1μM of PGE_2 (Cayman Chemical, Ann Arbor, Michigan, USA), and 10μM of Cay10526 (Cayman Chemical, Ann Arbor, Michigan, USA) and incubated with *P. brasiliensis*. To determine the killing rate, after 48 h, the cells were lysed with saponin (0.05%) and plated in BHI. The CFUs were counted after 7–14 days. Nitrite production in the culture supernatants of the killing assay or culture with 2.10^5 BMDMs from WT and *Nlrc4*$^{-/-}$ nontreated or treated was estimated using the Griess reaction.

Lung cell isolation and flow cytometry

Lung cells were isolated as described previously (Souza et al., 2018; Tristão et al., 2017). Briefly, the lung was digested in 1 mL of digestion buffer (2mg/mL collagenase IV [Sigma-Aldrich] and 1mg/mL DNase [Sigma-Aldrich]). Lung fragments were filtered with 50-μm nylon screens (BD Biosciences) and centrifuged (200*g*, 10 min, 4°C). Pellets were washed with lysis buffer and resuspended in RPMI with 5% FBS. Viable cells (10^6) were stimulated with 50 ng/mL PMA (Sigma-Aldrich) and 500ng/mL Ionomycin and 1μL of Brefeldin A (BioLegend) for 4 h at 37°C. Fixed cells (4% PBS-formalin) were permeabilized using PBS containing 1% FBS, 0.1% sodium azide, and 0.2% saponin. Staining was performed with the fluorochrome-conjugated antibodies. The following antibodies were used: CD3 (1:100; clone: 145-2C11); CD4 (1:100; clone: RM4-4); CD8 (1:100; clone: 53-6.7); CD45 (1:100; clone: 30-F11); CD11b (1:100; clone: M1/70); CD11c (1:100; clone: N418); I-A/I-E (1:100; clone: M5/114.5.2); Ly6C (1:100; clone: HK1.4); Ly6G (1:100; clone 1A8); IFN-γ (1:200; clone: XM 61.2); IL-1β (1:200; clone: NJTEN3); perforin (1:200; clone: eBioOMAK-D); granzyme B (1:200; clone:GB11); and granzyme-A (1:200; clone: 3G8.5). Antibodies were purchased from BioLegend (San Diego, CA), eBioscience (Waltham, Massachusetts, EUA), and BD Biosciences (Franklin Lakes, New Jersey, USA). Data acquisition was performed with a FACSCanto II (BD Biosciences, San Diego, CA). Data were analyzed using FlowJo software v.10.0.8 (Tree Star, Inc, Ashland, OR). Gating hierarchy is shown in Figures S1D, S1F, and S4B.

Indomethacin treatment

The indomethacin treatment with BMDMs and *P. brasilinesis*-infected mice as previously described (Michelin et al., 2002; Zoccal et al., 2016), respectively. Briefly, BMDMs were pretreated during 2 h with indomethacin (10μM) before incubation with Pb18. Mice were pretreated 1 day before and once a day after Pb18 infection with indomethacin via intraperitoneal route (2mg/Kg). Controls were treated with indomethacin vehicle (Tris[hydroxymethyl]aminomethane-HCl; pH 8.2). Schematic representation of the treatment with indomethacin is shown in Figure 4D

PGE_2 quantification

$PGE_2$was quantified in lung homogenates via liquid chromatography-mass spectrometry (LC-MS/MS) as described previously (Sorgi et al., 2017). Briefly, lipids were extracted using methanol and C18 solid-phase columns. Samples were submitted to LC-MS/MS analysis using the TripleTOF^R 5600+ system (AB Sciex – Foster, CA, USA).

MCC950 treatment

The MCC950 (InvivoGen, San Diego, CA, USA) (Nlrp3 inflammasome inhibitor) treatment in mice was adapted from the study by Tate et al. (2016). Briefly, *P. brasiliensis*-infected mice were treated with MCC950 via intranasal route (1mg/Kg, 50uL) at 15 dpi with one day interval per treatment. Controls (vehicle) were treated with saline buffer. Schematic representation of the treatment with MCC950 is shown in Figure 6A.

QUANTIFICATION AND STATISTICAL ANALYSIS

Statistical analysis

Data were normally distributed. Significant differences between experimental groups were evaluated with one-way ANOVA and Bonferroni multicomparison test or student's t-test. The log-rank test (Mantel–Cox) was used to evaluate survival curves. Error bars depict mean ± SD. Analyses were performed with GraphPad Prism software v8.2.1 (GraphPad Software Inc., San Diego, CA, EUA). Statistical significance was set at $p < 0.05$.